Contrast enhancement by lipid-based MRI contrast agents in mouse atherosclerotic plaques : a longitudinal study

CONTRAST MEDIA & MOLECULAR IMAGING

Received: 6 March 2012, Revised: 27 July 2012, Accepted: 3 August 2012, Published online in Wiley Online Library

(wileyonlinelibrary.com) DOI: 10.1002/cmmi.1496

Contrast enhancement by lipid-based MRI contrast agents in mouse atherosclerotic plaques; a longitudinal study

Brigit den Adel[a], Linda M. van der Graaf[a], Ivo Que[b], Gustav J. Strijkers[c], Clemens W. Löwik[b], Robert E. Poelmann[a] and Louise van der Weerd[a,d,e]*

The use of contrast-enhanced MRI to enable *in vivo* specific characterization of atherosclerotic plaques is increasing. In this study the intrinsic ability of two differently sized gadolinium-based contrast agents to enhance atherosclerotic plaques in ApoE$^{-/-}$ mice was evaluated with MRI. We obtained a kinetic profile for contrast enhancement, as the literature data on optimal imaging time points is scarce, and assessed the longer-term kinetics. Signal enhancement in the wall of the aortic arch, following intravenous injection of paramagnetic micelles and liposomes, was followed for 1 week. *In vivo* T_1-weighted MRI plaque enhancement characteristics were complemented by fluorescence microscopy of NIR_{664} incorporated in the contrast agents and quantification of tissue and blood Gd–DTPA. Both micelles and liposomes enhanced contrast in T_1-weighted MR images of plaques in the aortic arch. The average contrast-to-noise ratio increased after liposome or micelle injection to 260 or 280% respectively, at 24 h after injection, compared with a pre-scan. A second wave of maximum contrast enhancement was observed around 60–72 h after injection, which only slowly decreased towards the 1 week end-point. Confocal fluorescence microscopy and whole body fluorescence imaging confirmed MRI-findings of accumulation of micelles and liposomes. Plaque permeation of contrast agents was not strongly dependent on the contrast agent size in this mouse model. Our results show that intraplaque accumulation over time of both contrast agents leads to good plaque visualization for a long period. This inherent intraplaque accumulation might make it difficult to discriminate passive from targeted accumulation. This implies that, in the development of targeted contrast agents on a lipid-based backbone, extensive timing studies are required. Copyright © 2012 John Wiley & Sons, Ltd.
Supporting information may be found in the online version of this paper

Keywords: atherosclerosis; kinetics; MRI; paramagnetic contrast agents

1. INTRODUCTION

Atherosclerotic disease remains the primary cause of mortality in industrialized countries, despite the clinical advances that have been made in the prevention and treatment of this disease over the past 20 years (1). Studies have shown that more than two-thirds of acute coronary syndromes occur in patients who are classified as being at intermediate risk according to traditional Framingham Score risk-stratification methods. Based on these findings, it is clear that noninvasive diagnostic strategies are required to accurately assess the extent of cardiovascular disease in order to predict which patients most urgently need treatment.

High-resolution magnetic resonance imaging (MRI) has emerged as one of the most promising techniques for the direct and non-invasive evaluation of atherosclerotic plaques (2–5). The natural differences in tissue structure between the healthy vessel wall and atherosclerotic lesions result in contrast differences on T_{1w}, T_{2w} and DW MRI scans (6). However, particularly in the early stages, discriminating intimal thickening and developing lesions from healthy vessels is not straightforward because of the limited sensitivity, partial volume effects and motion artifacts inherent to these scans.

Apart from the afore-mentioned 'traditional' MR imaging approaches, there is increasing interest in the use of MR contrast agents that enable a more refined characterization of atherosclerotic plaques (7,8). Dynamic contrast-enhanced imaging using small gadolinium-based contrast agents such as gadofluorine (9,10) and gadodiamide (11) has been explored to investigate plaque neo-vascularization and permeability. Although the above studies

* *Correspondence to: L. van der Weerd, Leiden University Medical Center, Department of Radiology, PO Box 9600, 2300 RC Leiden, The Netherlands. Email: L.van_der_Weerd@lumc.nl*

a *B. den Adel, L. M. Graaf, R. E. Poelmann, L. van der Weerd*
Department of Anatomy and Embryology, Leiden University Medical Center, Leiden, the Netherlands

b *I. Que, C. W. Löwik*
Department of Endocrinology, Leiden University Medical Center, Leiden, The Netherlands

c *G. J. Strijkers*
Biomedical NMR, Department of Biomedical Engineering, Eindhoven University of Technology, Eindhoven, the Netherlands

d *L. van der Weerd*
Department of Radiology, Leiden University Medical Center, Leiden, the Netherlands

e *L. van der Weerd*
Department of Human Genetics, Leiden University Medical Center, Leiden, the Netherlands

have demonstrated that imaging of plaques and even intraplaque processes is feasible in patients, these Gd chelates still have an inherently low relaxivity ($r_1 \approx 3.4\,mmol^{-1}\,s^{-1}$ at 1 T), resulting in only a modest signal enhancement.

A number of strategies have been developed to amplify the relaxivity and to deliver sufficient quantities of Gd *in vivo* in order to detect atherosclerotic lesions. One of these strategies is to use lipid-based nanoparticles like micelles or liposomes, carrying high payloads of amphipathic Gd chelates embedded in the outer lipid membrane. These particles may contain as many as 50 000 Gd atoms, resulting in a relaxivity per particle that is magnitudes higher than of single Gd chelates (12). Other previously explored approaches for contrast-enhanced MRI of atherosclerotic plaque include perfluorcarbon nanoparticles (13) and iron oxide particles (14).

Lipid-based nanoparticles like micelles and liposomes accumulate in atherosclerotic plaques owing to a leaky vasculature, ineffective lymphatic drainage and enhanced endocytotic activity. This phenomenon provides a mechanism for passive targeting of nanoparticles to atherosclerotic sites (15). The MR contrast agents used in this paper are polyethylene glycol2000 (PEG2000) micelles and liposomes that include gadolinium diethylenetriamine pentaacetic acid (Gd–DTPA) based lipids (16,17). This platform has been used to image macrophages in plaques and oxidized low-density lipoprotein (LDL). These nanoparticles have a longer half-life than regular micelles (18,19) owing to the protective 'stealth' effect of the outer shell of PEG chains, which reduces recognition by opsonins and consequently clearance (18), resulting in increased accumulation at inflamed sites (20,21).

The pharmacokinetics of these nanoparticles and the resulting concentration gradient between blood and atherosclerotic lesion determines the wash-in and wash-out kinetics, and thereby the timing of maximum contrast enhancement of the plaque (20,22). In practice, contrast-enhanced MRI using nanoparticles is typically performed at baseline and either followed for a short period of time (a few hours) or measured at a single time point within 1–48 h after contrast agent administration. Data on the optimal imaging time points are scarce (23,24). Even though the pharmacokinetics of larger liposomes, iron oxides and perfluorcarbon nanoparticles has been extensively studied (25–27), very little is known about the dynamics of contrast enhancement of micelles and liposomes in atherosclerotic plaque during longer periods of time. Longitudinal follow-up of plaque development and therapy response through imaging is highly desirable and for that purpose Gd-loaded micelles and liposomes are more frequently applied. In this respect, detailed information on the accumulation and clearance kinetics of contrast agents is of major importance.

In this study, we therefore aimed (1) to obtain a kinetic profile for contrast enhancement and (2) to assess the longer-term kinetics of Gd-loaded micelles and liposomes. We assessed the passive kinetic behavior of Gd-loaded micelles and liposomes in atherosclerotic plaques in the aortic arch of 1-year-old $ApoE^{-/-}$ mice over a period of 1 week using MRI and plasma profiles. Liposomes and micelles were labeled with a fluorescent marker for validation of the MRI finding using histology and for *in vivo* whole-body biodistribution measurements.

2. MATERIALS AND METHODS

2.1. Hardware

All experiments were performed with a vertical 9.4 T magnet (Bruker, Ettlingen, Germany) supplied with an actively shielded Micro2.5 gradient system of $1\,T\,m^{-1}$ and a 30 mm transmit/receive birdcage RF coil, using Paravision 4.0 software.

2.2. Contrast Agents

Micelles and liposomes were prepared by lipid film hydration as described previously (28). A mixture of the appropriate amounts of lipids (typically 120 mol of total lipid) was dissolved in chloroform–methanol 3:1 (v/v) in a round-bottom flask. A lipid film was made under reduced pressure using rotary evaporation at 37 °C and dried under a stream of nitrogen. For micelles Gd–DTPA–BSA [Gd–DTPA–bis(stearylamide)] and PEG2000-DSPE {1,2-distearoyl-sn-glycero-3-phosphoethanolamine-*N*-[methoxy (polyethyleneglycol)-2000]} were used at a molar ratio of 1.5:1.35. For fluorescent detection, 0.1 mol% NIR664-DSPE (SyMO-CHEM B.V., Eindhoven, The Netherlands) was added. The lipid film was subsequently hydrated in HEPES buffered saline (HBS), containing 20 mM HEPES and 135 mM NaCl (pH 7.4) and vigorously stirred at 65 °C for 45 min.

For liposomes, Gd–DTPA–BSA (Gd–DTPA–bis(stearylamide), DSPC (1,2-distearoyl-sn-glycero-3-phosphocholine), cholesterol and PEG2000-DSPE were used at a molar ratio of 0.75:1.10:1:0.15 and rehydrated in HBS as described for micelles. The resulting lipid dispersion was extruded sequentially four times through polycarbonate membrane filters (Nuclepore, Pleasanton, CA, USA) with a pore diameter of 200 nm and subsequently 10 times through filters with a pore diameter of 100 nm using a Lipofast Extruder (Avestin, Canada). The temperature during extrusion was 65 °C.

The size and size distribution of the contrast agents were determined by dynamic light scattering (DLS) at 25 °C with a Malvern 4700 system (Malvern ZetaSizer Nano S, Malvern, UK). The micelles had a mean size of 16 nm and liposomes had a mean size of 100 nm. Both micelles and liposomes had a polydispersity index <0.1, which indicates a narrow size distribution. The relaxivity was measured at 37 °C and 9.4 T. The phospholipid content of the liposome preparations was determined by phosphate analysis according to Rouser after destruction with perchloric acid (29). pH stability was assessed using DLS at different pH, ranging from 4.0 to 9.0.

2.3. *In vivo* Experiments

All experiments were conducted in accordance with the Dutch guidelines for research animal care at our institution. A schematic overview of the experimental design and groups of mice ($n = 34$) can be found in Fig. 1. Each block in this figure represents an experimental group.

Thirty-four groups ($n = 5$ per group) of aged (between 10 and 14 months old) male $ApoE^{-/-}$ mice on a C57BL/6/J background were fed a normal chow diet. For MRI and assessment of contrast agent distribution, 30 groups were used: each mouse was scanned before administration of contrast agent and every 6 h for 142 h (6 days) after intravenous injection of the equivalent of 50 μmol Gd^{3+}–DTPA lipid kg^{-1} bodyweight (i.e. 1.25 μmol Gd per 25 g body weight) in 200 μl micelles or liposomes (Fig. 1). Mice were anesthetized during MRI with isoflurane (±2% in oxygen and air). At every 6 h time-point until 30 h post injection, a group of mice ($n = 5$) was taken out of the experiment and killed by transcardial perfusion for histological validation of MRI images. After 30 h, groups of mice were taken out of the experiment every 12 h. In total 16 groups of mice for both

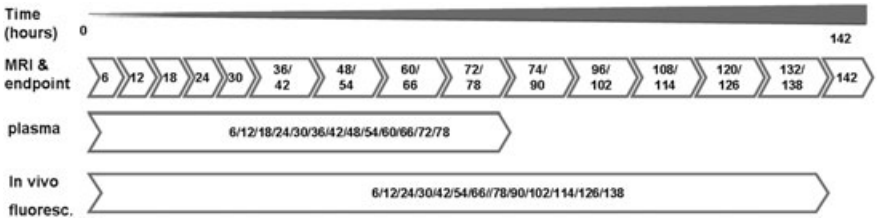

Figure 1. A schematic overview of the *in vivo* experiments showing the distribution of different groups of animals over the experiments. Each block represents a group of five animals that is sacrificed at the end time indicated in the box.

micelles and liposomes were used to monitor the *in vivo* behavior of these nanoparticles.

Two separate groups of mice were used to follow kinetics of the contrast agents in blood. Moreover, for *in vivo* fluorescent imaging, two groups of mice were used.

2.4. MRI Protocols

2.4.1. *In vivo*

At the start of each examination, several 2D FLASH scout images were recorded in the transverse and axial planes through the heart to determine the orientation of the aortic arch. A modified FLASH sequence with a navigator echo (IntraGate) was used for retrospective CINE MRI with the following parameters:

(1) Cross sections of the aortic arch – RF pulse 1 ms; flip angle 15°; repetition time (*TR*) 31.4 ms; echo time (*TE*) 2.96 ms; navigator echo points 64; 10 cardiac frames; field of view $1.8 \times 1.8\,cm^2$; matrix 128×128; in-plane resolution $141 \times 141\,\mu m^2$; six slices, slice thickness 0.4 mm; number of repetitions 400; total acquisition time approximately 20 min.
(2) For a frontal view of the aortic arch, the MR sequence was slightly adapted – *TR* 15.7 ms, *TE* 2.96 ms, three slices, slice thickness 0.5 mm, total acquisition time approximately 10 min.

During the examination, the respiration rate was continuously monitored using a balloon pressure sensor connected to the ECG/respiratory unit. The isoflurane concentration was adjusted to keep the respiration rate between 50 and 90 respirations per minute.

2.4.2. *Ex vivo*

Blood samples were drawn from the tail vein from $n = 5$ mice for both micelle and liposome injected mice every 6 h for 78 h. T_1 values of plasma samples were determined using a saturation recovery protocol spin-echo sequence with the following parameters: *TE* 7 ms; *TR* 25, 20, 15, 10, 8, 6, 5, 4, 3, 2, 1.6, 1.2, 1.0, 0.8, 0.6, 0.4 and 0.3 s; matrix 128×128; resolution $195 \times 195\,\mu m^2$; two slices; slice thickness 1 mm.

The T_1 values of the various regions of interest (ROIs) were determined using the three-parameter fit function:

$$M(t) = M0\,(1 - \exp[-t/T_1]) \tag{1}$$

The change in longitudinal relaxation rate ΔR_1 values of the blood over time were determined by:

$$\Delta R_1(t) = (1/T_1[\mathrm{Gd}(t)]) - 1/T[0] \tag{2}$$

The ΔR_1 values were fitted using a mono-exponential decay function

$$\Delta R_1(t) = Ae^{-\ln(2)t/t_{1/2}} \tag{3}$$

where A is the initial quantity of gadolinium, and $t_{1/2}$ is the circulation half-life of gadolinium in the blood.

2.5. MRI Analysis

Images were analyzed using ImageJ software. Black blood images in three to four adjacent slices of cross-sections through the aortic arch were analyzed. ROIs were drawn around the plaque region in the vessel wall (I_{wall}). A second ROI was drawn in the surrounding muscle tissue of the shoulder girdle (I_{muscle}). Furthermore, an ROI was placed outside the animal to measure the noise level ($stdev_{noise}$) (Fig. 2).

The contrast–to-noise ratio (CNR) was defined as

$$\mathrm{CNR} = (I_{wall} - I_{muscle})/\mathrm{stdev}_{noise}, \tag{4}$$

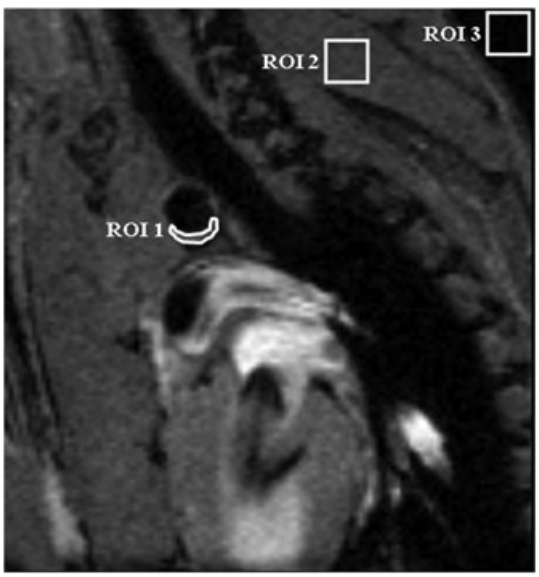

Figure 2. Contrast-to-noise ratios of atherosclerotic plaques were determined in black blood images of a cross-section of the aortic arch by region of interest (ROI) 1, the signal intensity of the plaque in the vessel wall (I_{wall}) corrected on ROI 2, the signal intensity of surrounding muscle tissue (I_{muscle}) and ROI 3, the standard deviation of the noise ($stdev_{noise}$).

which is a measure of how well the lesioned wall can be discriminated from the surrounding tissue. CNR values are shown as means ± standard deviation.

2.6. Optical Imaging

Whole body distribution of NIR664 was followed for 7 days at 12 h intervals using 700 nm laser excitation (IVIS spectrum). OptiView software was used to create both intensity and lifetime images and a pixel-to-pixel ROI comparison.

2.7. Gd–DTPA ELISA

Gd–DTPA concentrations in tissue homogenates of liver, kidney, lungs and the aortic arch were determined using an enzyme immunoassay test kit (BioPAL Inc., Huissen, The Netherlands) with a sensitivity limit of 0.5 pg. Tissue samples (lungs, liver, kidney, spleen, heart, aortic arch) from five mice per contrast agent per time point were harvested at 6, 12, 18, 24, 30, 48 and 60 h after contrast agent injection.

2.8. Histology

Aortic arches were frozen in Tissue Tek® (Sakura Finetek Europe, Zoetermeer, The Netherlands) and cut into serial 5 μm sections. Sections were stained with Oil Red O for lipid deposition and hematoxilin eosin for gross morphology, followed by bright-field microscopy.

To detect the presence of F4-80 positive macrophages, sections were fixed in 10% isopropanol and incubated overnight at room temperature with a rat polyclonal primary antibody against F4-80 (1:100, SantaCruz). Rabbit anti rat conjugate (1:200, DAKO) with normal rabbit serum diluted in PBS was incubated for 1 h at room temperature as a secondary antibody. Biotin labeling was followed by development using DAB (Vector Laboratories Inc., UK) and counterstaining was performed with Mayer's hematoxilin. Sections were analyzed using bright-field microscopy.

Imaging of micelle and liposome fluorescence was performed using a Leica TCS-SL confocal laser scanning microscope interfaced to a DM6000B microscope. NIR_{664} was excited with a 633 nm HeNe laser; emission was filtered through a band-pass filter of 650–710 nm. Autofluorescence of elastic lamellae was detected at an emission wavelength of 450–500 nm.

2.9. Statistical Analysis

Data are presented as the means ± standard deviation. Statistical analysis was performed using SPSS 15.0 ANOVA for computations within and between groups. Results were considered statistically significant at $p < 0.05$.

3. RESULTS

3.1. Nanoparticle Characteristics

The manufactured nanoparticles were characterized using DLS, showing that the micelles had a mean hydrodynamic diameter of approximately 16 nm with a polydispersity index of 0.1, indicating a narrow size distribution. Liposomes were approximately 5- to 6-fold larger than micelles, with a mean diameter of 100 ± 0.05 nm. Micelles had a higher r_1 relaxivity per mmol Gd compared to liposomes (Table 1), at both 1.41 and 9.4 T at 37 °C and pH 7.3. For liposomes it was already known that they are stable within a physiological pH range (30). Micelles were tested for stability with changing pH; decreasing the pH did not compromise micelle stability. Decreasing the pH to 4.0 resulted in only a very modest change in size distribution from 16 to 15.4 nm. Increasing the pH to 9.0, however, resulted in increased hydrodynamic diameter of micelles, which may be explained by the hypertonicity of the solvent.

3.2. *In vivo* MRI Study

In line with contrast agent concentrations applied in previous studies (16,31), $ApoE^{-/-}$ mice were injected intravenously with a single dose of contrast agent at a concentration of 50 μmol Gd^{3+}–DTPA lipid per kg bodyweight. Axial and sagittal T_{1w} images of the aortic arch were made before contrast agent injection, as well as directly after contrast agent administration. Scans were repeated at several time points after injection, for up to 24 h. T_1-weighted MRI images showed a strong bright blood effect after an intravenous bolus injection of liposomes or micelle. The blood enhancement gradually disappeared during the 24 h after injection owing to clearance of the particles from the blood stream. Contrast enhancement was analyzed by drawing regions of interest on plaque areas at the basis of the aortic arch in black blood images (Fig. 2). Average CNR increased gradually after liposome or micelle injection to 260 or 280%, respectively, at 24 h after micelle injection when compared with the pre-scan (Fig. 3A). Very early timepoints are shown in more detail in supplementary Figure 1. However, the CNR had not reached a plateau at 24 h post injection, which led us to postulate that micelles and liposomes were still circulating and entering atherosclerotic plaques after these time points.

Therefore, the fluctuations in CNR were monitored over time for a longer period of 1 week after injection, both for micelles and liposomes (Fig. 3B). One day after contrast agent injection, the signal intensities of both nanoparticles started to drop significantly. However, a second contrast enhancement peak was observed at around 60–72 h after injection, which only slowly decreased towards the 1 week post injection end-point. The area in the vessel wall with clear contrast enhancement was larger at the second peak contrast point than within the first 24 h after administration (Fig. 3B).

Table 1. Contrast agent properties

	Hydrodynamic diameter (nm)			r_1 ($mM^{-1} s^{-1}$)	
	pH7.3	pH 4.0	pH 9.0	1.4 T, 37 °C	9.4 T room temp
Micelles	16.1 ± 0.2	15.4	20.2	11.4	5.8
Liposomes	103 ± 0.4	101 ± 0.2	121 ± 0.9	6.5	2.5

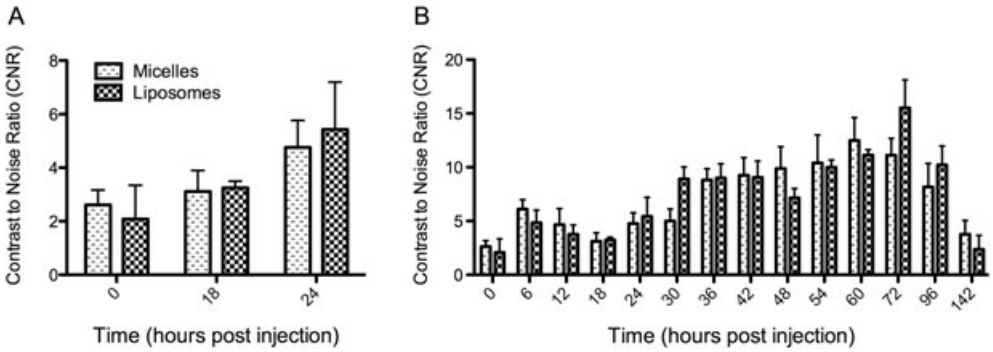

Figure 3. Contrast-to-noise ratios (CNR) of atherosclerotic plaques were determined at different time points after micelle or liposome injection and plotted against time. (A) CNR follow-up until 24 h post injection; (B) CNR follow-up for several days.

3.3. Plasma Kinetics

Plasma T_1 values were determined to assess the amount of circulating contrast agent, using blood samples obtained from the tail vein taken at regular intervals after contrast agent injection. Plasma T_1 values showed an inverse relation to the fluctuations in CNR observed in atherosclerotic plaques (Fig. 4A). Shortly after contrast agent injection, a sharp decrease in plasma T_1 was observed, which slowly increased to almost normal plasma T_1 values between 10 to 30 h after injection. Thereafter, a second decrease in T_1 values was observed for both contrast agents, which was more prominent in the case of micelles.

Based on the ΔR_1 values during the first 24 h (before recirculation), the blood circulation half-life was calculated to be 8.1 h for micelles (R^2 =0.95) and 5.3 h (R^2 =0.96) for liposomes, assuming mono-exponential behavior (Fig. 4B).

3.4. *In vivo* Detection of Whole Body Biodistribution

To further assess the pharmacokinetics of the nanoparticles, we measured the biodistribution with *in vivo* fluorescence imaging using the NIR_{664} fluorochrome incorporated in the lipid layer of the respective nanoparticles. In line with the enhancement pattern observed with MRI, contrast agent accumulation was observed in the region of the aortic arch, with maximum accumulation around 40 and 60 h after injection for micelles and liposomes respectively (Fig. 5). However, a biphasic pattern in fluorescence, like that detected with MRI in the aortic arch region, could not be observed. In the first 15 min after injection, both the renal and hepatic regions became positive, indicative of primary accumulation and/or elimination via that route. Steady, but slowly fading, accumulation in the neck region (maybe the carotid arteries) and axillary lymph nodes was observed over the entire measurement period of 7 days. Apart from the expected uptake and clearance routes, the paws of all animals that were injected with micelles and liposomes showed NIR_{664} fluorescence, possibly indicative of poor circulation in the paws of these aged mice. Excretion of the fluorescent dye was observed in the feces, confirming the involvement of the liver in the metabolism of the contrast agents.

3.5. Assessment of Gadolinium Content

An enzyme-linked immunosorbent assay (ELISA), originally developed for the detection of Gd–DTPA in serum and urine, was performed on tissue homogenates from internal organs harvested every 6 h after contrast agent injection, i.e. directly after MRI at the respective time points. The ELISA was used to indirectly determine the biodistribution of micelles and liposomes via Gd–DTPA in liver, lungs, kidney, spleen, aortic arch and heart 6 h after contrast agent injection. We observed Gd accumulation in the liver of about 4 and 7% of the injected dose (ID) and in the spleen of about 2 and 3% of ID for micelles and liposomes, respectively. The lungs and kidney showed less accumulation, in the order of 0.5–1% of the ID after 6 h (Fig. 5). In all these organs, Gd was cleared over the 60 h of the experiment. In contrast, both the heart and the aortic arch showed an initial decrease in gadolinium content followed by a steady secondary increase in Gd during the second to third day after injection, consistent with the contrast increase observed on MRI (Fig. 6).

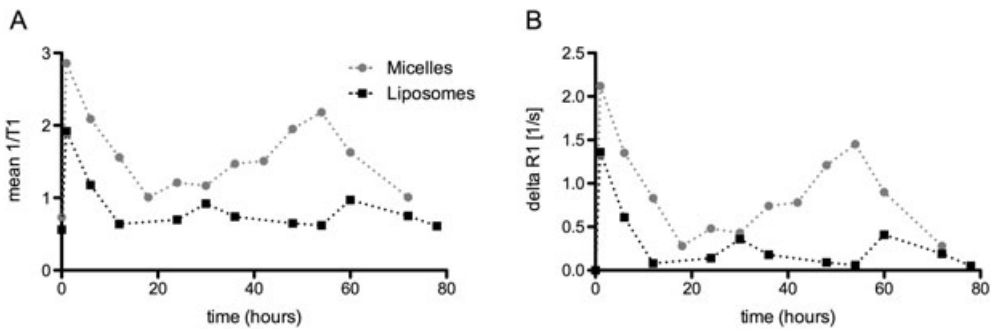

Figure 4. $1/T_1$ values in (A) describe the inverted pattern of micelle and liposome blood circulation compared with the accumulation patterns observed in the aortic arch. In (B) the temporal changes in R_1 values illustrate the blood circulation and circulation half-life calculated over the first 24 h.

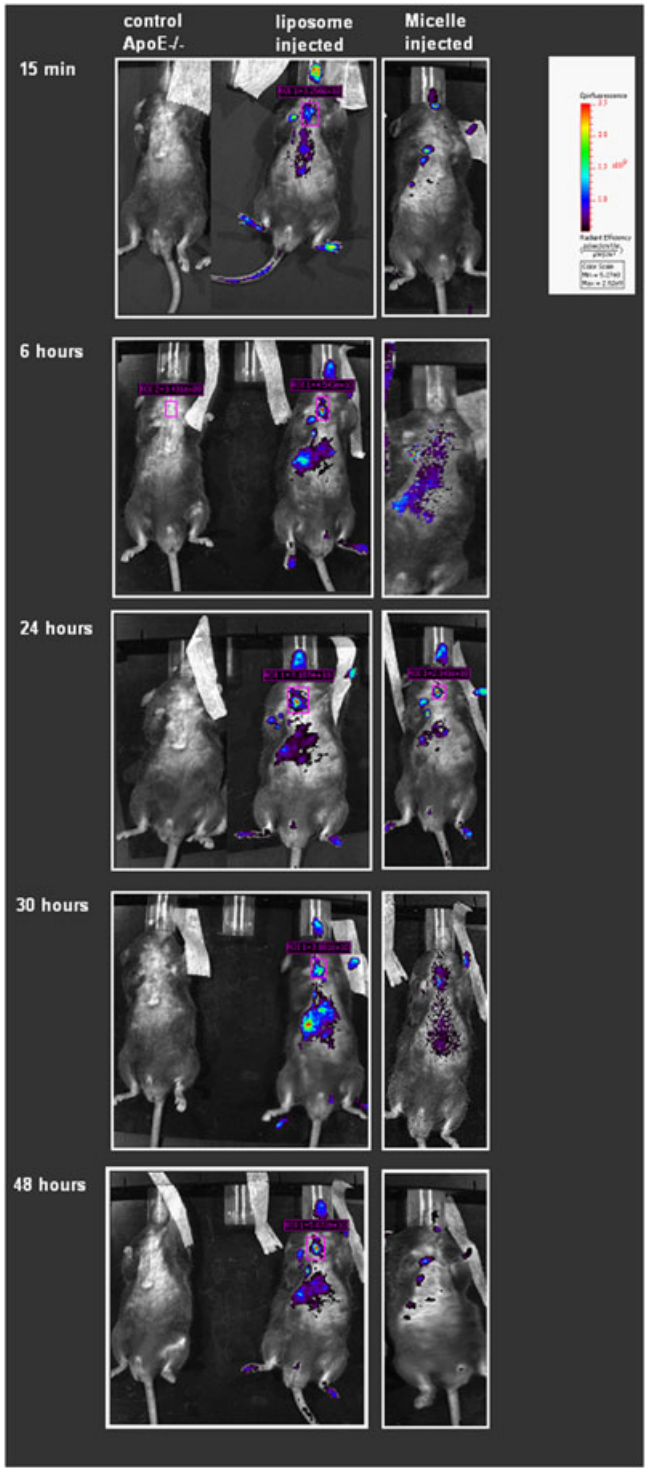

Figure 5. Whole body fluorescence imaging of ApoE$^{-/-}$ mice after injection of liposomes or micelles shows the distribution patterns over time of the NIR_{664} fluorophore incorporated in the contrast agents.

3.6. Immunohistochemistry

To examine which components within atherosclerotic plaques are preferably targeted by micelles and liposomes, confocal laser scanning microscopy and light microscopy were performed on cryosections of the aortic arch. For confocal laser scanning microscopy, elastic lamellae were autofluorescent in the green spectrum; liposomes and micelles were already labeled with NIR_{664}.

Early after contrast agent injection, at 12 h, the presence of contrast agents within atherosclerotic plaques could be confirmed (Fig. 7). However, at this time no uptake of the nanoparticles in the macrophages or macrophage-derived foam cells could be observed. At later time points, starting 24 h after injection, it was observed that liposomes were mainly found associated with elastic lamellae, whereas this was not the case for micelles (Fig. 7). Micelles were found in macrophage-positive areas from 12 h after injection onwards. Staining for smooth-muscle cells with α-actin did not show any micelle or liposome uptake in these cells (data not shown). This suggests that liposomes remain restricted to the extracellular space of the atherosclerotic plaque and that there was no cellular uptake of the contrast agent, whereas micelle retention is linked to the presence of macrophages. Some colocalization was observed for the elastic lamellae and the micelles in the atherosclerotic plaque. Although in all sections micelles and liposomes were found throughout the entire aortic plaque, the contrast agents were heterogeneously distributed, with most micelles and liposomes present in the center of the plaque early after injection, but in the cap regions of the plaque at later time points.

4. DISCUSSION

4.1. Biphasic Enhancement on MRI

In this study we determined the pharmacokinetics of untargeted lipid-based Gd-loaded micelles and liposomes in the ApoE$^{-/-}$ atherosclerotic mouse. ApoE$^{-/-}$ mice are characterized by the spontaneous and diet-induced occurrence of atherosclerosis in their arteries at sites with low and oscillatory flow patterns (8). The occurrence of atherosclerotic plaques is preceded by damage to the endothelial layer, rendering the endothelium leaky. As a consequence molecules, but also nanoparticles like micelles and liposomes, can pass the endothelial lining and penetrate atherosclerotic plaques where they may be retained.

Here we show that, in the unaffected vessel wall, no MR contrast enhancement occurred, whereas at the classical atherosclerosis-prone sites increased signal intensity was observed with peak contrast enhancement at two time points around 12 and around 60 h after injection in ApoE$^{-/-}$ mice. Previous studies already mention peak contrast points shortly after injection (minutes), which can be attributed to a first passage effect and peak enhancements in the period of 12–24 h after contrast agent injection, with contrast agent follow-up ranging from 24 to 48 h (24,32). The difference between the previous results and our recent observations may be attributed to imaging timing (much later time points than previously) and possibly also increased sensitivity to the detection of contrast enhancement by the use of cine MRI.

This biphasic kinetic pattern was present for both liposomes and micelles. For all time points, the areas of MRI contrast enhancement showed good agreement with the Gd–DTPA concentration in tissues and the presence of NIR664 on the histological sections, suggesting that the paramagnetic and fluorescent lipids remain co-localized for the entire observation period.

During the second wave of enhancement, we still observed co-localization of the fluorescence and Gd signal. When contrast agents are administered intravenously there may be some local

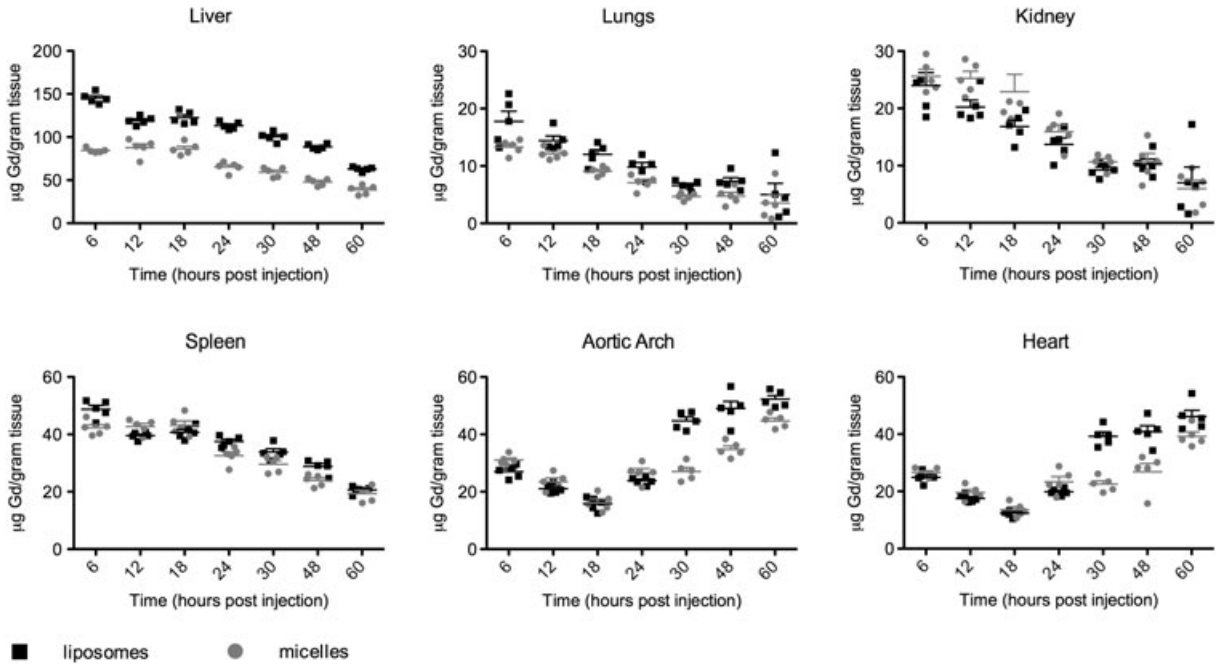

Figure 6. Gd–DTPA accumulation was determined at several time points by ELISA on tissue homogenates in liver (A), lungs (B), kidneys (C), spleen (D), heart (E) and aortic arch (F). An increase in Gd–DTPA can be observed in the hearts and aortic arch of animals injected with both micelles and liposomes starting around 30 h post injection.

extravasation encouraged by mass action, owing to particle size and loading dose. The second contrast wave may also be due to slow release of these particles from the liver, or more likely from contrast agent-loaded macrophages migrating out of the spleen in the days following contrast agent injection, as previously observed with ^{19}F in the early days of RES imaging (33). At this time point, the micelles and liposomes were probably no longer intact, but one could easily interpret the results differently because we did not observe differences in the time course or localization within the plaque of the fluorescent and Gd components based on the histological evaluation. Whether or not the particles were still intact, this second contrast wave should be considered for longitudinal experiments, as it will be a confounding factor in follow-up studies.

4.2. Passive Accumulation in Plaques: micelles vs Liposomes

From the microscopic analysis, it became apparent that the uptake mechanism of micelles in atherosclerotic plaque was most likely related to passive diffusion of the micelles over the abnormal endothelial lining followed by uptake into phagocytic cells like monocytes and macrophages. Liposomes were also found inside the plaque, but mainly outside cells and close to the elastic laminae.

No significant liposome or micelle uptake was observed in normal vessel walls of ApoE$^{-/-}$ mice with MRI or histology. LSCM showed a predominant first uptake of the contrast agents into the extracellular space of the plaque on the laminar side of the lesion in ApoE$^{-/-}$ mice, indicative of the enhanced permeability of the vessel wall. Furthermore, colocalization of the micelles with cell nuclei and F4-80-positive cells revealed that micelles were retained in the plaque by uptake in cells, whereas this was not the case for liposomes. We did not observe ingestion of the nanoparticles within circulating monocytes or macrophages in the first hours after injection, as determined by blood smears. This, however, does not rule out that ingestion does occur at a low percentage and that these cells then migrate into the plaque.

Finally, maximum signal enhancement of the plaque occurred at relatively late time points suggestive of slow uptake and accumulation of both liposomes and micelles in the plaque. The difference in behavior inside the plaque of the particles may be due to the difference in size, which makes it favorable to phagocytose micelles but not liposomes (34).

4.3. Clearance and Distribution Pathways

During the first phase after injection, contrast agents that were cleared from the blood accumulated in various organs, as shown by the *in vivo* whole body biodistribution studies and the Gd-content in tissue homogenates. Both micelles and liposomes are metabolized through the liver and to a much lesser extent by the kidneys. The liver may serve as a reservoir for the nanoparticles as the fluorescence and Gd–DTPA content remains high over time and clearance from this organ is slow. Compared with micelles, liposomes accumulated more in the spleen, liver and lungs of mice, possibly owing to the fact that liposomes are an order of magnitude larger than micelles and therefore get trapped in the capillary beds in these organs. At atherosclerotic areas this difference disappears as the damaged endothelial lining of atherosclerotic layer allows easier passage of particles. Both in micelle- and in liposome-injected mice, a steady decline in Gd content in the spleen was observed, which suggests involvement of the spleen in the redistribution of the Gd lipids.

We did not observe a biphasic enhancement pattern for the aortic plaques in the *in vivo* fluorescence study. However, this

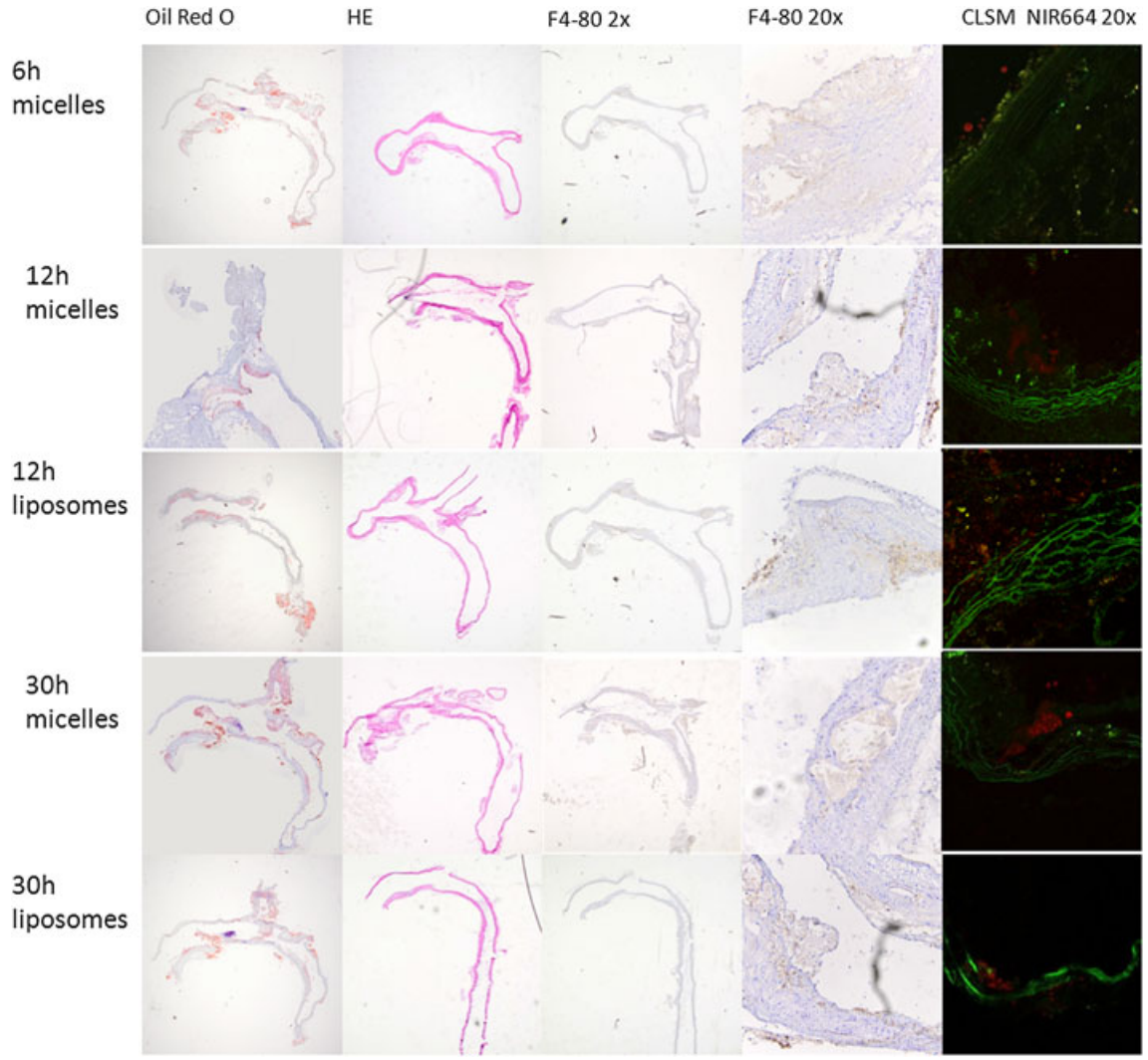

Figure 7. Histology of aortic arch after contrast agent injection. Lipid deposition in vessel wall is visualized with Oil Red O, and gross morphology with hematoxilin eosin. Presence of macrophages in the plaques is visualized via F4-80. NIR664 in contrast agents is visualized in corresponding plaque regions on adjacent histological slices.

does not imply that it is not present. On MRI images we report differences in T_1 in the plaque with high sensitivity and spatial accuracy, and thereby indirectly on the fluctuations in the amount of contrast agent internalized in the plaque. In contrast, specific quantification of the fluorescent signal in the aortic arch was not possible owing to the low spatial resolution of *in vivo* fluorescence cameras and the relatively large amount of micelle and liposome uptake in the entire thoracic region (i.e. in the heart, lymph nodes and large arteries). As reported previously, liposomes and micelles did not produce a sufficient signal to visualize the plaques in its anatomical context *in vivo*, presumably because of insufficient tissue penetration of the exciting and emitted signals (35). *Ex vivo* visualization of the aortic arch, however, showed increased fluorescence in the aortic tree and at the basis of the aortic arch in line with our histological findings. Overall we observed no real differences in tissue distribution between micelles and liposomes, which is in line with previous studies using other nanoparticles (26,27,32,36).

5. CONCLUSIONS

The maximum enhancement for Gd-loaded micelles and liposomes was shown to be dependent on contrast agent size and blood circulation kinetics, which underscores that plaque enhancement by nontargeted and targeted contrast agents must be interpreted with care. Our results indicate that the timing of contrast-enhanced MRI is of utmost importance and will need to be optimized for every novel contrast agent and animal model.

Supporting Information

Supporting information can be found in the online version of this article.

REFERENCES

1. Sanz J, Moreno PR, Fuster V. The year in atherothrombosis. J Am Coll Cardiol 2008; 51(9): 944–955.

2. Choudhury RP, Fuster V, Fayad ZA. Molecular, cellular and functional imaging of atherothrombosis. Nat Rev Drug Discov 2004; 3(11): 913–925.
3. Itskovich VV, Samber DD, Mani V, Aguinaldo JG, Fallon JT, Tang CY, et al. Quantification of human atherosclerotic plaques using spatially enhanced cluster analysis of multicontrast-weighted magnetic resonance images. Magn Reson Med 2004; 52(3): 515–523.
4. Ruehm SG, Corot C, Vogt P, Kolb S, Debatin JF. Magnetic resonance imaging of atherosclerotic plaque with ultrasmall superparamagnetic particles of iron oxide in hyperlipidemic rabbits. Circulation 2001; 103(3): 415–422.
5. Yuan C, Hatsukami TS, Cai J. MRI plaque tissue characterization and assessment of plaque stability. Stud Health Technol Inform 2005; 113: 55–74.
6. Sanz J, Fayad ZA. Imaging of atherosclerotic cardiovascular disease. Nature 2008; 451(7181): 953–957.
7. Saraste A, Nekolla SG, Schwaiger M. Cardiovascular molecular imaging: an overview. Cardiovasc Res 2009; 83(4): 643–652.
8. Van der Heiden K, Hierck BP, Krams R, De CR, Cheng C, Baiker M, et al. Endothelial primary cilia in areas of disturbed flow are at the base of atherosclerosis. Atherosclerosis 2008; 196(2): 542–550.
9. Barkhausen J, Ebert W, Heyer C, Debatin JF, Weinmann HJ. Detection of atherosclerotic plaque with Gadofluorine-enhanced magnetic resonance imaging. Circulation 2003; 108(5): 605–609.
10. Sirol M, Itskovich VV, Mani V, Aguinaldo JG, Fallon JT, Misselwitz B, et al. Lipid-rich atherosclerotic plaques detected by gadofluorine-enhanced in vivo magnetic resonance imaging. Circulation 2004; 109(23): 2890–2896.
11. Kerwin WS, O'Brien KD, Ferguson MS, Polissar N, Hatsukami TS, Yuan C. Inflammation in carotid atherosclerotic plaque: a dynamic contrast-enhanced MR imaging study. Radiology 2006; 241(2): 459–468.
12. Mulder WJ, Strijkers GJ, van Tilborg GA, Griffioen AW, Nicolay K. Lipid-based nanoparticles for contrast-enhanced MRI and molecular imaging. NMR Biomed 2006; 19(1): 142–164.
13. Tran TD, Caruthers SD, Hughes M, Marsh JN, Cyrus T, Winter PM, et al. Clinical applications of perfluorocarbon nanoparticles for molecular imaging and targeted therapeutics. Int J Nanomedicine 2007; 2(4): 515–526.
14. Burtea C, Laurent S, Mahieu I, Larbanoix L, Roch A, Port M, et al. In vitro biomedical applications of functionalized iron oxide nanoparticles, including those not related to magnetic properties. Contrast Media Mol Imag 2011; 6(4): 236–250.
15. Peer D, Karp JM, Hong S, Farokhzad OC, Margalit R, Langer R. Nanocarriers as an emerging platform for cancer therapy. Nat Nanotechnol 2007; 2(12): 751–760.
16. Mulder WJ, Strijkers GJ, Briley-Saboe KC, Frias JC, Aguinaldo JG, Vucic E, et al. Molecular imaging of macrophages in atherosclerotic plaques using bimodal PEG-micelles. Magn Reson Med 2007; 58(6): 1164–1170.
17. Mulder WJ, Griffioen AW, Strijkers GJ, Cormode DP, Nicolay K, Fayad ZA. Magnetic and fluorescent nanoparticles for multimodality imaging. Nanomedicine (Lond) 2007; 2(3): 307–324.
18. Lukyanov AN, Torchilin VP. Micelles from lipid derivatives of water-soluble polymers as delivery systems for poorly soluble drugs. Adv Drug Deliv Rev 2004; 56(9): 1273–1289.
19. Torchilin VP. Structure and design of polymeric surfactant-based drug delivery systems. J Control Release 2001; 73(2–3): 137–172.
20. Chono S, Tauchi Y, Deguchi Y, Morimoto K. Efficient drug delivery to atherosclerotic lesions and the antiatherosclerotic effect by dexamethasone incorporated into liposomes in atherogenic mice. J Drug Target 2005; 13(4): 267–276.
21. Metselaar JM, Storm G. Liposomes in the treatment of inflammatory disorders. Expert Opin Drug Deliv 2005; 2(3): 465–476.
22. Neubauer AM, Sim H, Winter PM, Caruthers SD, Williams TA, Robertson JD, et al. Nanoparticle pharmacokinetic profiling in vivo using magnetic resonance imaging. Magn Reson Med 2008; 60(6): 1353–1361.
23. Klink A, Lancelot E, Ballet S, Vucic E, Fabre JE, Gonzalez W, et al. Magnetic resonance molecular imaging of thrombosis in an arachidonic acid mouse model using an activated platelet targeted probe. Arterioscler Thromb Vasc Biol 2010; 30(3): 403–410.
24. Beilvert A, Cormode DP, Chaubet F, Briley-Saebo KC, Mani V, Mulder WJ, et al. Tyrosine polyethylene glycol (PEG)-micelle magnetic resonance contrast agent for the detection of lipid rich areas in atherosclerotic plaque. Magn Reson Med 2009; 62(5): 1195–1201.
25. McGoron AJ, Pratt R, Zhang J, Shiferaw Y, Thomas S, Millard R. Perfluorocarbon distribution to liver, lung and spleen of emulsions of perfluorotributylamine (FTBA) in pigs and rats and perfluorooctyl bromide (PFOB) in rats and dogs by ^{19}F NMR spectroscopy. Artif Cells Blood Substit Immobil Biotechnol 1994; 22(4): 1243–1250.
26. Waters EA, Chen J, Yang X, Zhang H, Neumann R, Santeford A, et al. Detection of targeted perfluorocarbon nanoparticle binding using ^{19}F diffusion weighted MR spectroscopy. Magn Reson Med 2008; 60(5): 1232–1236.
27. Waters EA, Chen J, Allen JS, Zhang H, Lanza GM, Wickline SA. Detection and quantification of angiogenesis in experimental valve disease with integrin-targeted nanoparticles and 19-fluorine MRI/MRS. J Cardiovasc Magn Reson 2008; 10: 43.
28. Mulder WJ, Strijkers GJ, Griffioen AW, Van BL, Molema G, Storm G, et al. A liposomal system for contrast-enhanced magnetic resonance imaging of molecular targets. Bioconjug Chem 2004; 15(4): 799–806.
29. Rouser G, Fkeischer S, Yamamoto A. Two dimensional then layer chromatographic separation of polar lipids and determination of phospholipids by phosphorus analysis of spots. Lipids 1970; 5(5): 494–496.
30. Sabin J, Prieto G, Ruso JM, Hidalgo-Alvarez R, Sarmiento F. Size and stability of liposomes: a possible role of hydration and osmotic forces. Eur Phys J E Soft Matter 2006; 20(4): 401–408.
31. Briley-Saebo KC, Amirbekian V, Mani V, Aguinaldo JG, Vucic E, Carpenter D, et al. Gadolinium mixed-micelles: effect of the amphiphile on in vitro and in vivo efficacy in apolipoprotein E knockout mouse models of atherosclerosis. Magn Reson Med 2006; 56(6): 1336–1346.
32. van Bochove GS, Paulis LE, Segers D, Mulder WJ, Krams R, Nicolay K, et al. Contrast enhancement by differently sized paramagnetic MRI contrast agents in mice with two phenotypes of atherosclerotic plaque. Contrast Media Mol Imag 2011; 6(1): 35–45.
33. Ratner AV, Hurd R, Muller HH, Bradley-Simpson B, Pitts W, Shibata D, et al. 19F magnetic resonance imaging of the reticuloendothelial system. Magn Reson Med 1987; 5(6): 548–554.
34. Roerdink F, Wassef NM, Richardson EC, Alving CR. Effects of negatively charged lipids on phagocytosis of liposomes opsonized by complement. Biochim Biophys Acta 1983; 734(1): 33–39.
35. Peters D, Kastantin M, Kotamraju VR, Karmali PP, Gujraty K, Tirrell M, et al. Targeting atherosclerosis by using modular, multifunctional micelles. Proc Natl Acad Sci USA 2009; 106(24): 9815–9819.
36. Mulder WJ, Strijkers GJ, Briley-Saboe KC, Frias JC, Aguinaldo JG, Vucic E, et al. Molecular imaging of macrophages in atherosclerotic plaques using bimodal PEG-micelles. Magn Reson Med 2007; 58(6): 1164–1170.

